

# Dynamic Wireless Power Transfer System with Twin Perpendicular Receiver Coils

(Invited Paper)

Heng-Ming Hsu<sup>1</sup>, Bo Yang<sup>2,\*</sup>, Tai-Lai Yang<sup>1</sup>, Hsin-Lin Cho<sup>1</sup>, and Naoki Shinohara<sup>2</sup>

<sup>1</sup>Electrical Engineering Department, National Chung Hsing University, Taichung 402-27, Taiwan

<sup>2</sup>Research Institute for Sustainable Humanosphere, Kyoto University, Uji 611-0011, Japan

**ABSTRACT:** Wireless power transfer (WPT) with dynamic charging capabilities is a promising technology that can charge moving objects in real-time. However, maintaining high-efficiency power transfer during vehicle movement continues to be a significant challenge. To address this challenge, this study proposes a dynamic WPT system that utilizes orthogonal transmitter and receiver coils, offering the advantages of stable output power and efficiency, even when the vehicle is in motion. Unlike other systems, the proposed topology eliminates the need for a complicated feedback control system, thereby reducing hardware costs. To verify the effectiveness of the proposed topology, a dynamic WPT system was implemented in this study. Measurement results demonstrate that even when the vehicle moves a distance of 400 mm (four times the length of the receiving coil), the output voltage and power variations are only 4.9% and 9.6%, respectively.

## 1. INTRODUCTION

Industrial smart manufacture factories use machines and tools to automate various applications. However, using cables for power supply can limit the freedom of operation for these machines and tools. This has led to the recent research on wireless power transfer (WPT) technology, which completely eliminates the need for wires [1–3]. Automatic material handling system is one of the most widely used systems in the industry. In a clean smart factory room, overhead hoist transport (OHT) is often used to carry manufacturing materials using a rail-guided vehicle, as shown in Fig. 1 (<https://www.muratec.net/cfa/products/>). The rail-guided vehicle and the track form a dynamic WPT system. It is crucial that the dynamic WPT provides consistent performance when the vehicle is moving to maintain high-efficiency and deliver a constant output power.

To implement dynamic WPT for vehicles moving along a track, Pacini et al. [4] used many control switches, which increased the hardware cost. Another approach is to use a transmitter to supply a long, straight track, but it leads to decreased coupling among coils and results in low transfer efficiency, as seen in the current OHT system. Additionally, the use of a long track can cause the transmitter to deliver unstable power [5]. Smeets et al. constructed an array by connecting multiple transmitter coils in parallel [6]. However, this structure has a null-point problem at the junction of a transmitter coil, resulting in large power variations at the receiver and increasing the DC-DC converter cost. Therefore, Zhou and Mi proposed several

paralleled LCC reactive power compensation networks to regulate the current in the primary coil to reduce the system's power loss [7].

To address the aforementioned issues, a perpendicular topology of transmitter and receiver coils has been proposed in the literature [8]. This topology completely eliminates the null problem, as there is no mutual inductance in the vertical direction. However, in this previous study, the authors only proposed a single receiver coil and focused on its coil behavior. In this work, a twin receiver coil perpendicular to the transmitter coil is proposed to increase the received magnetic field, considering that the magnetic field is an intrinsic closed loop. The coil topologies of the  $XY$ - and  $XZ$ -planes are illustrated in Figs. 2(a) and 2(b), respectively. Fig. 2(b) shows the twin receiver coils positioned at the top and bottom to facilitate the reception of the magnetic field delivered by the transmitter. The transmitter coil consists of four identical coils connected in parallel to construct the track.

It is worth noting that we employ a single inverter to drive four transmitter coils, and the coil length can be extended as needed for practical applications. The fundamental concept here is the use of one inverter to drive multiple coils. The receiver coil embedded in the moving vehicle uses two coils with opposite current directions across the transmitter to acquire additional magnetic field delivered from the transmitter coil. As a result, the receiver coils are mechanically aligned with the transmitter coil. Consequently, environmental factors do not affect this work.

To validate the proposed topology, a dynamic WPT system was implemented to measure the output voltage and power during vehicle movement. The results show that the vehicle can

\* Corresponding author: Bo Yang (yang\_bo@rsh.kyoto-u.ac.jp).

Invited paper for the Commemorative Collection on the 150-Year Anniversary of Maxwell's Equations.

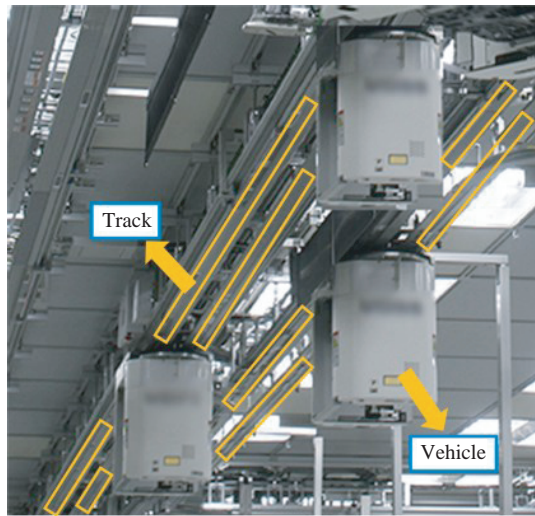


**FIGURE 1.** Application scenario of the proposed dynamic WPT. An overhead hoist transport (OHT) system that is implemented on tracks and vehicles.

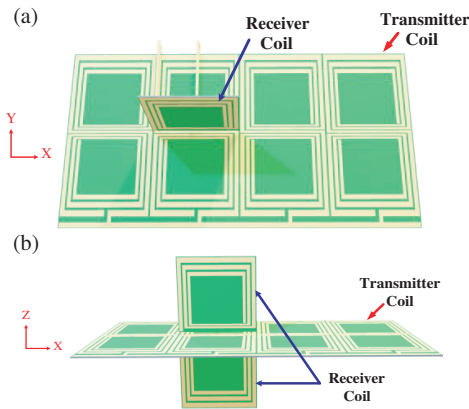


**FIGURE 2.** Illustration of proposed dynamic WPT coil topology. Orthogonal transmitter (Tx) and receiver (Rx) coils are depicted in two side views. (a) XY-plane. (b) XZ-plane.

move a distance of 400 mm with only 4.9% and 9.6% variations in output voltage and power, respectively.

This paper is organized as follows. In Section 2, we analyze the proposed coil characteristics to maintain a fixed mutual inductance during movement, ensuring that the transmitter delivers constant voltage and power to the receiver. Section 3 presents the design mindset and optimization of the receiver coil. Section 4 discusses the integration of the system to work at high efficiency and the realization of the hardware to demonstrate the proposed topology. Finally, in Section 5, we present a brief conclusion.

## 2. ANALYSIS ON MUTUAL INDUCTANCE

In the evaluation of a wireless power transfer system, the most critical parameters are transmission efficiency and the power delivered to the load. To achieve wireless power transfer technology in a dynamic system where the coupling coils are designed on the track and vehicle to ensure simultaneous charg-

ing during movement, the system adopts inductive coupling. However, as the vehicle moves along the track, the mutual inductance changes due to the changing position of the coupling coil. Therefore, maintaining a stable mutual inductance in a moving object is crucial. In the following paragraph, we will characterize the mutual inductance of both traditional and proposed topologies.

### 2.1. Traditional Topology

Figure 3 illustrates the structure of a traditional coil [11], which consists of four sub-coils with a side length of  $l$ , line width of  $w$ , and distance between two sub-coils of  $s$  connected in parallel to form the transmitter (Tx) coil. The dimension of the receiver (Rx) coil is identical to the transmitter sub-coil, and it is aligned with the transmitter coil with a vertical distance of  $h$ . It should be noted that the movement direction of the receiver coil is along the  $X$ -axis. To analyze the total inductance comprehensively between the stationary transmitter coil and the moving receiver coil, the transmitter coil of each line segment is denoted as B1-B4, T1-T4, and 1-8, whereas the receiver coil is labeled as  $a$ - $d$  in Fig. 3. The total inductance is calculated using (1).

$$L_{total} = L_{TX} + L_{RX} + \sum_{i=1}^8 (M_{ai} + M_{ci}) + \sum_{i=1}^4 [(M_{bTi} + M_{bBi}) + (M_{dT_i} + M_{dB_i})] \quad (1)$$

where  $L_{TX}$  and  $L_{RX}$  represent the self-inductance of transmitter and receiver coils, respectively, and are not affected by the position of the receiver. The mutual inductance between line segments  $b$  and  $d$ , and line segments T1-T4 and B1-B4 is expressed as the summation of  $M_{bTi} + M_{dB_i}$ . When the distance between the transmitter sub-coils is small ( $s \cong 0$ ), T1-T4 and B1-B4 can be considered as long straight wires (Ti and Bi), and segments  $b$  and  $d$  can be treated as moving along these two long straight wires (Ti and Bi).

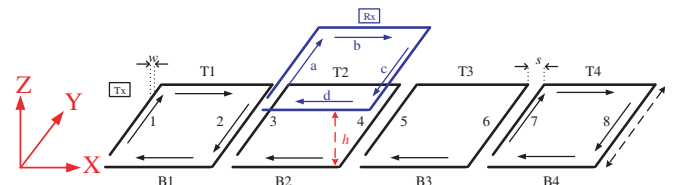


**FIGURE 3.** Brief diagram of a traditional coil topology. The transmitter sub-coil has a width of  $w$  and a length of  $l$ . The space between two transmitter sub-coils is  $s$ , the distance between transmitter and receiver is  $h$ . The name of each line segment: symbols of  $a$ - $d$  are four segments of receiver; symbols of 1-8 are segments in the  $Y$ -axis of transmitter; symbols of T1-T4 and B1-B4 are in the  $X$ -axis direction of transmitter. The arrow direction shows the current flow of each line segment.

To facilitate the following discussion, the position of the receiver coil in Fig. 4 is defined as follows: when the receiver coil is not yet entered the first transmitter sub-coil, its position

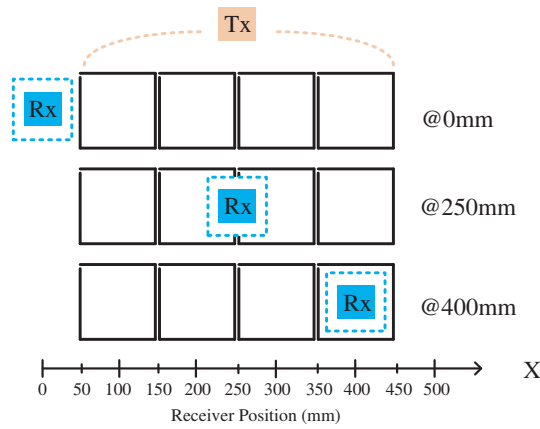


**FIGURE 4.** Definition of receiver position. When the receiver coil has not entered the first transmitter sub-coil, its position is defined as  $X = 0$ ; when the receiver coil is between the second and third transmitter sub-coils, its position is  $X = 250$  mm; when the receiver coil is located at the fourth transmitter sub-coil, its position is  $X = 400$  mm.

is  $X = 0$ ; when the coil is between the second and third transmitter sub-coils, its position is  $X = 250$  mm; when the receiver coil is on the fourth transmitter sub-coil, its position is  $X = 400$  mm.

Next, we analyze the mutual inductance between the receiver coil of line segments  $b$  and  $d$  and the transmitter coil. Based on the simulation results, the mutual inductance between the receiver coil of line segments  $b$  and  $d$  and the transmitter coil is found to have a variation about 5% when the receiver coil moves a distance of 400 mm along the track. This means that the mutual inductance is relatively stable even when the receiver coil is in motion, which is an essential requirement for achieving high-efficiency power transfer in a dynamic WPT system. Additionally, it is observed that the transmitter coil does not change significantly during the movement of the receiver coil.

In Figs. 5(a) and (b), the traditional coil topology is shown in  $XZ$ -plane views when the receiver is positioned at  $X = 200$  mm and  $X = 250$  mm, respectively. It can be observed that the distance between the receiver (segments  $a$  and  $c$ ) and transmitter coils (segments 1 and 8) is notably different. For instance, as the receiver moves from  $X = 200$  mm to  $X = 250$  mm, the length between receiver segment  $a$  and transmitter segment 3 changes from  $h$  to  $\sqrt{h^2 + 0.25(l + d - w)^2}$ . Simultaneously, the length between receiver segment  $a$  and transmitter segment 4 is also changing, as shown in Fig. 5(b).

As mutual inductance is strongly dependent on the distance between two segments,  $M_{ai}$  and  $M_{ci}$  values change significantly with the movement of the receiver. Therefore, these two mutual inductances are the main causes of variations when the receiver position changes. To better understand mutual inductance variations, we calculate them using equation [12], which gives the mutual inductances of two parallel segments as follows:

$$M = \frac{\mu_0}{2\pi} l \left[ \ln \frac{2l}{h} - 1 + \frac{h}{l} - \frac{1}{4} \frac{h^2}{l^2} \right] \quad (2)$$

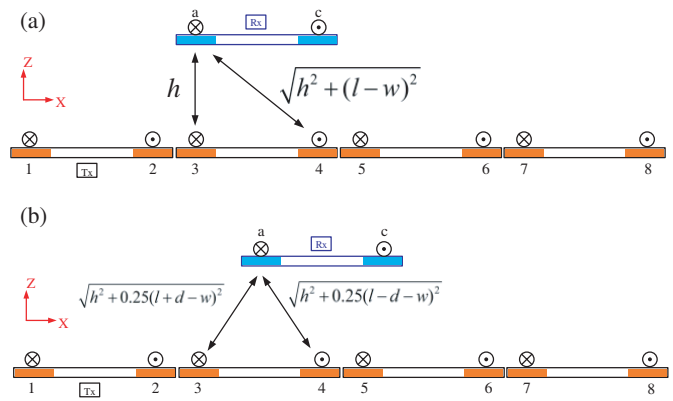


**FIGURE 5.**  $XZ$ -plane view of a traditional coil. (a) Receiver is located at  $X = 200$  mm. (b) Receiver is located at  $X = 250$  mm. The distance between line segments “ $a$ ” and “3” is named as  $\overline{a3}$  and similarly for other segments.

where  $l$  is the length,  $h$  the distance between two segments, and  $\mu_0$  the permittivity.

It is evident that mutual inductance mainly depends on the length  $l$  of the segment and the distance between two segments  $h$ . Thus, any change in the distance ( $h$ ) leads to a corresponding change in the mutual inductance. This is the main disadvantage of the traditional topology.

### 2.2. Proposed Topology

To eliminate mutual inductance variations, we needed to eliminate the mutual inductances between segments  $a$  and  $c$  of receiver and transmitter coils. Therefore, we erected the receiver coil to be perpendicular to the transmitter coil in this work. The mutual inductance vanishes because segments  $a$  and  $c$  are placed in a vertical position. It is worth noting that the magnetic field is a closed loop. Additionally, we placed another receiver coil with a contrary current direction directly below the transmitter coil to acquire an additional magnetic field, as depicted in Fig. 6.

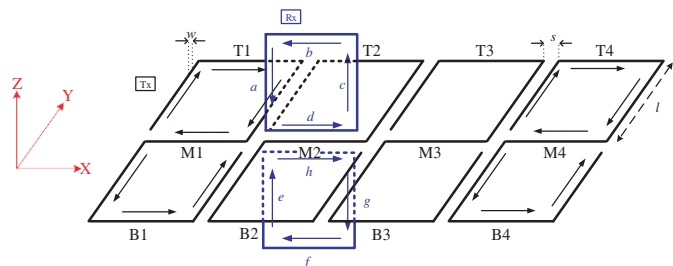


**FIGURE 6.** Brief diagram of the proposed coil topology. The entire transmitter array comprises four parallel sub-coils. Transmitter and receiver coils are orthogonal to each other, forming a closed loop of magnetic field. The transmitter sub-coil has a width of  $w$  and a length of  $l$ . The space between two transmitter sub-coils is  $s$ . The name of each line segment: symbols of  $a-h$  are eight segments of receiver; symbols of T1-T4, M1-M4, and B1-B4 are in the  $X$ -axis direction of transmitter. The arrow direction shows the current flow of each line segment.

Now, we calculate the overall equivalent inductance of the proposed topology using (3).

$$L_{total} = L_{TX} + L_{RX} + (M_{aTX} + M_{cTX} + M_{eTX} + M_{gTX}) + \sum_{i=1}^4 \left[ \begin{matrix} (M_{bTi} + M_{bMi} + M_{bBi}) \\ + (M_{dT_i} + M_{dM_i} + M_{dB_i}) \\ + (M_{fT_i} + M_{fM_i} + M_{fB_i}) \\ + (M_{hT_i} + M_{hM_i} + M_{hB_i}) \end{matrix} \right] \quad (3)$$

It is worth noting that the self-inductance of both  $L_{TX}$  and  $L_{RX}$  is not affected by the position of the receiver. In addition, the mutual inductance of segments  $a$ ,  $c$ ,  $e$ , and  $g$  of the receiver coil is perpendicular to all segments of the transmitter coil, resulting in an approximate mutual inductance of  $M_{aTX} + M_{cTX} + M_{eTX} + M_{gTX}$  to be zero. This solves the issue of segments  $a$  and  $c$  used to cause a significant variation in mutual inductance in the traditional topology.

If the distance between the transmitter sub-coils is small ( $s \cong 0$ ), then the segments T1-T4, M1-M4, and B1-B4 can be regarded as long straight wires  $T_i$ ,  $M_i$ , and  $B_i$ , respectively. Therefore, the summation item in (3) can be considered as the mutual inductance between segments  $b$ ,  $d$ ,  $f$ , and  $h$  and the three straight wires  $T_i$ ,  $M_i$ , and  $B_i$ . The total inductance can be expressed as follows:

$$L_{total} = L_{TX} + L_{RX} + (M_{bT} + M_{bM} + M_{bB}) + (M_{dT} + M_{dM} + M_{dB}) + (M_{fT} + M_{fM} + M_{fB}) + (M_{hT} + M_{hM} + M_{hB}) \quad (4)$$

The simulation of the magnetic field in the  $YZ$ -plane using EM software is shown in Fig. 7, indicating that the magnetic field is highly concentrated on the cross point of transmitter and receiver coils. The proposed topology utilizes the perpendicular placement of transmitter and receiver coils and their contrary current directions to yield a closed loop of magnetic field, resulting in an additional mutual inductance between transmitter and receiver coils.

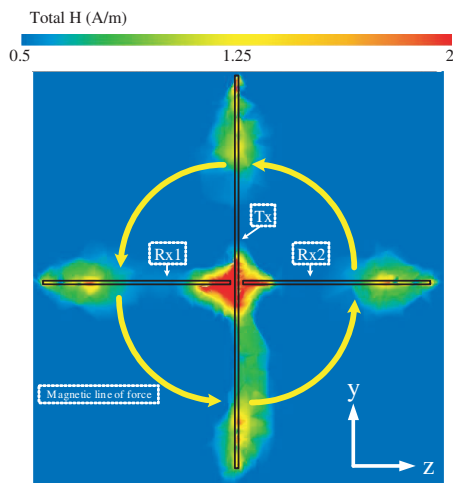


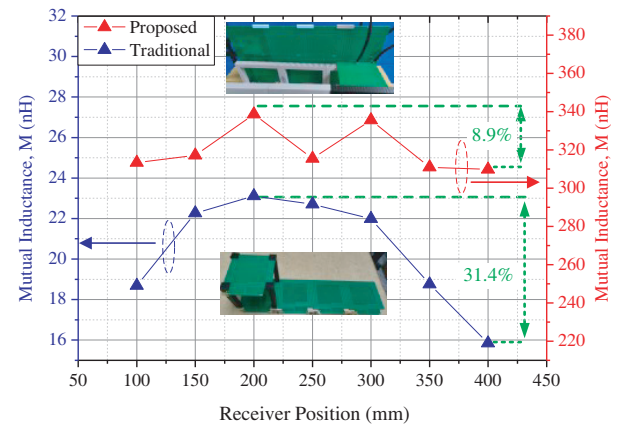
**FIGURE 7.** Magnetic field simulation in the  $YZ$ -plane of the proposed coil. Obviously, magnetic field is concentrated on the central region of transmitter (Tx) and receiver (Rx) coils.

The geometric dimensions were designed with a length ( $l$ ) of 98 mm and a width ( $w$ ) of 5 mm for the transmitter and receiver coils, with a spacing ( $s$ ) of 2 mm between transmitter coils and a distance ( $h$ ) of 10 mm between the two coils. To ensure a fair comparison between the traditional and proposed topologies, the distance between the transmitter and receiver coils was kept constant. These parameters were used to calculate the mutual inductances for both topologies, with an identical air gap. For convenient comparison, the mutual inductance variation was defined as follows:

$$M_{var} = \frac{2(M_{max} - M_{min})}{(M_{max} + M_{min})} \quad (5)$$

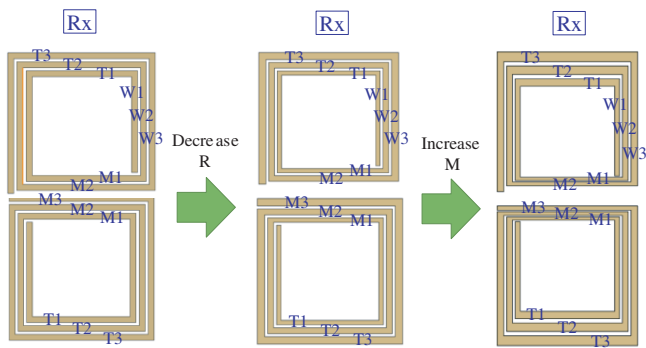
Equation (1) demonstrates that the total inductance is determined by both self-inductance and mutual inductance. The mutual inductance depends on the distance between the coils, which changes as the receiver coil moves. Fig. 8 illustrates the variation of mutual inductance with respect to the horizontal distance between the coils ( $X$ -axis).

Figure 8 shows the mutual inductance plotted against the receiver location for the measurement results. It is evident that the mutual inductance variations for the proposed and traditional topologies are 8.9% and 31.4%, respectively. The graph also demonstrates that the proposed twin receiver coils acquire a greater amount of magnetic field, with a measured mutual inductance of 320 nH compared to 20 nH for the traditional topology. This result is approximately 16 times larger in the proposed coil, verifying that the proposed topology not only maintains a stable mutual inductance, but also acquires a larger mutual inductance, as depicted in Fig. 7.



**FIGURE 8.** Measurements of mutual inductances at different receiver positions for traditional and proposed coils.

Obviously, the mutual inductance decreases as the horizontal distance increases for the traditional coil. This reduction in mutual inductance causes a decrease in power transfer efficiency. In contrast, the proposed topology maintains a relatively constant mutual inductance, ensuring stable efficient power transfer. Therefore, the proposed topology can overcome the limitation of the traditional coil and provide efficient and stable power transfer during vehicle movement.



**FIGURE 9.** Design mindset of the proposed coil. The receiver (Rx) coil is optimized from fixed width, varied width to dynamic width by decreasing parasitic resistance and increasing mutual inductance.

### 3. DESIGN OF DYNAMIC RECEIVER COIL LAYOUT

In this section, we focus on optimizing the coil layout to improve the coil transmission efficiency. The proposed receiver coil design is shown in Fig. 9. We adopt the traditional winding approach to maintain an equal line width of the coil. To decrease the coil metal resistance, we use the variable line width approach to improve the quality factor (Q) of the inductor [9]. Finally, we adopt the dynamic width approach to increase the mutual inductance between coils, which further improves the mutual inductance on the basis of the variable width approach. The widths of the receiver coil are denoted by W1-W3, T1-T3, and M1-M3 in Fig. 9, and their layout dimensions are listed in Table 1.

**TABLE 1.** Receiver coil dimensions of FixW, VaryW, and DynamicW layouts.

Layout	W1/T1/M1 (mm)	W2/T2/M2 (mm)	W3/T3/M3 (mm)
FixW	4.00/4.00/4.00	4.00/4.00/4.00	4.00/4.00/4.00
VaryW	3.43/3.43/3.43	4.00/4.00/4.00	4.61/4.61/4.61
DynamicW	3.43/5.15/2.29	4.00/5.99/2.66	4.61/6.92/3.07

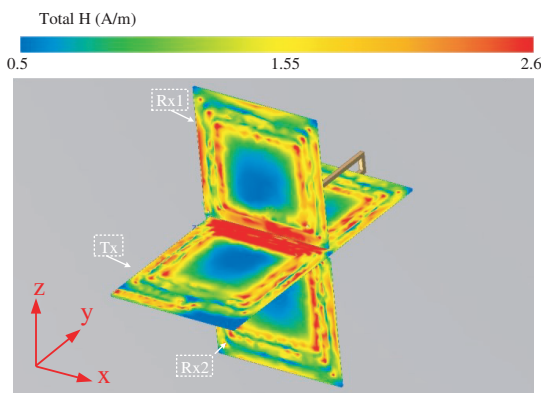


**FIGURE 10.** Diagram of magnetic field color temperature of the proposed coil. It shows that the magnetic field is concentrated on the central region of transmitter and receiver coils.

As shown in Fig. 6, line segments  $d$  and  $h$  of the receiver coil are the closest to the  $M_i$  line segment of the transmitter coil. Checking (4), the mutual inductances of  $M_{dM_i}$  and  $M_{hM_i}$  dominate the total mutual inductance. Notably, the current direction of line segments  $T_i$  and  $B_i$  is opposite to that of  $M_i$ . To increase mutual inductance, we use a small metal spacing in the center of the coil. The magnetic field color temperature graph of the dynamic width coil is shown in Fig. 10, and it demonstrates that the magnetic field is concentrated in the center area of the coil, indicating that the proposed layout is promising.

Finally, we compare the efficiencies of the three coil layouts in Fig. 11. The horizontal axis represents the receiver position, and the vertical axis represents the efficiency at a receiver height ( $h$ ) of 10 mm. The dynamic width layout improves efficiency by approximately 2.5% compared to the other two layouts.

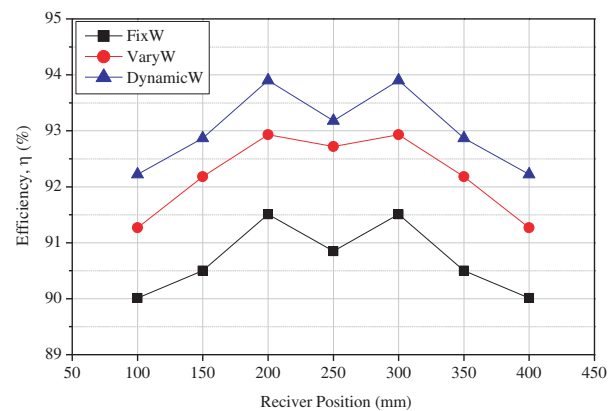


**FIGURE 11.** Comparison of efficiency versus receiver position for three layouts. The highest efficiency is achieved in dynamic width design.

### 4. DYNAMIC WPT SYSTEM INTEGRATION

In this section, we discuss the system diagrams of the proposed dynamic wireless power transfer (WPT) system. Fig. 12(a) illustrates the transmitter coil placement where one inverter (Tx) drives four transmitter coils that are connected in parallel to create a transmitter coil array. To reduce metal wire losses, we use the parallel topology instead of the series connection in the transmitter coil design. We add a resonant capacitor that resonates with the entire transmitter array to minimize the losses. The array number is dependent on the track length. To validate the proposed structure, a hardware-based WPT system is implemented, which comprises an inverter, four transmitter coils, one receiver coil, and a rectifier. This system operates at 13.56 MHz.

In order to determine the optimal trade-off between transmission efficiency and transistor cost, we have established an index based on the ratio of the length of the receiver (Rx) coil to the total length of the transmitter (Tx) coil. The unit coil cost is calculated as shown in Equation (6),

$$\text{Unit Coil Cost} = \frac{l_{RX}}{N \times l_{TX}} \quad (6)$$

where  $l_{TX}$  represents the length of a single Tx sub-coil,  $l_{RX}$  the length of the Rx coil, and  $N$  the number of sub-coils in one

**TABLE 2.** Average efficiency for different unit movement cost and number of sub-coils in a Tx array.

Efficiency	Unit coil cost	Sub-coil No. ( $N$ )
95%	1	1
93%	0.5	2
92.5%	0.25	4
87.5%	0.125	8
80%	0.0625	16

Tx array. For simplicity in this paper, we have chosen identical lengths for Tx and Rx coils, simplifying the unit movement cost to  $1/N$ .

Table 2 presents the relationship between unit movement cost and transmission efficiency. Notably, the efficiency experiences a significant drop from 92.5% to 87.5% as the unit cost decreases from 0.25 to 0.125. In summary, the efficiency remains nearly constant within the range of 92.5% to 95% as the unit coil cost decreases from 1 to 0.25.

To minimize costs, we have opted for four sub-coils ( $N = 4$ ) connected in parallel to form an array of Tx coils. These four sub-coils are simultaneously driven by a single inverter, reducing transistor costs by a factor of 4. The average efficiency achieved is approximately 92.5%.

The receiver coil is illustrated in Fig. 12(b) and is perpendicular to the transmitter coil. The receiver coil consists of two series of coils with opposite current directions to capture additional magnetic field delivered from the transmitter coil. The receiver coil (Rx) is connected to a rectifier circuit, which is embedded inside a moving vehicle. After designing the coupling coil, the maximum efficiency can be calculated to be 94% [10], and the corresponding optimum load should be matched to the input impedance of the receiver. This study integrates an inverter, a pair of coils, and a rectifier to ensure that each block operates in a high-efficiency region.

The schematic of the proposed dynamic WPT system is shown in Fig. 13. Transistors ( $M_1, M_2$ ) and capacitors ( $C_{p1}, C_{p2}$ ) construct two half-bridge class-E inverters. The inductors ( $L_{p1}, L_{p2}$ ) are the choke inductors. A control signal with a phase difference of 180 degrees is applied to each gate terminal of the two transistors to build a full-bridge class-E inverter. The topology delivers twice the output power with high efficiency. Class-E topology has high efficiency characteristics, which is an important parameter for wireless power transfer systems. The inductor ( $L_{TX}$ ) represents the four parallel coils at the transmitter node, while the inductor ( $L_{RX}$ ) represents the receiver coil.

To convert the AC power into DC power and supply it to the load, we use a class-D rectifier in the receiver circuit as shown in Fig. 13. The diodes ( $D_1$ - $D_4$ ) perform full-bridge rectification. When the operating frequency is high, the diode must switch quickly, and an imaginary impedance occurs at the rectifier input. We simulate and calculate the high-frequency impedance variation in the ADS simulator and draw it as an impedance trace on the Smith chart. The entire WPT system is

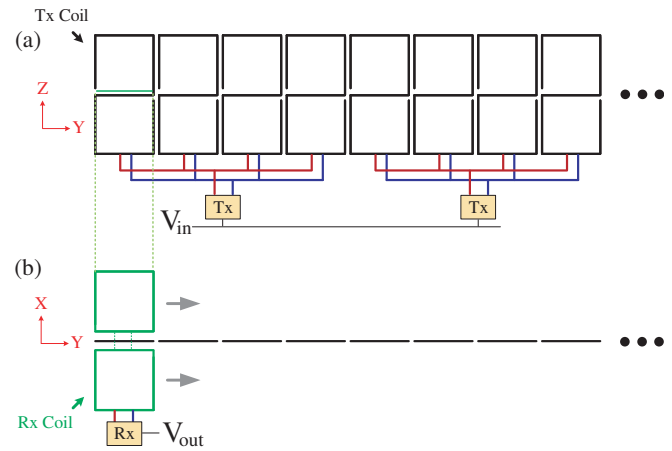


**FIGURE 12.** Brief block diagram of the proposed dynamic WPT system. The transmitter (Tx) array consists of four parallel sub-coils, which are driven by a single inverter. The number of sub-coils in the array can be extended to build a track. The receiver (Rx) has two coils perpendicular to the transmitter array, and a rectifier is connected to deliver output DC power.

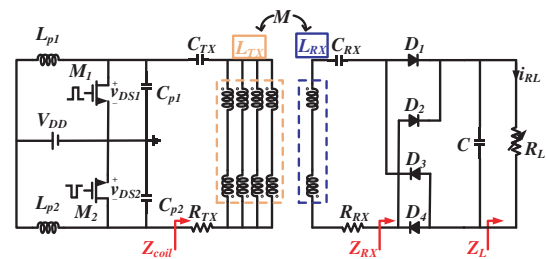


**FIGURE 13.** Schematic of the proposed dynamic wireless power transfer (WPT) system. The system consists of a transmitter coil and a dynamic receiver coil. The transmitter coil is connected to a resonant capacitor and a full-bridge inverter. The receiver coil is connected to a full-bridge rectifier and a DC load.

powered by the class-E inverter, which is suitable for operation in MHz and can achieve 100% theoretical efficiency. The maximum efficiency of the inverter can be obtained using rigorous circuit analysis.

The coil input impedance ( $Z_{coil} = R_{coil} + jX_{coil}$ ) can be derived from the T-model equivalent circuit. The real and imaginary parts of the input impedance are acquired as follows:

$$R_{coil} = \frac{(\omega M_{12})^2 (R_{rx} + R_2)}{(R_{rx} + R_2)^2 + X_{rx}^2} + R_1 \quad (7)$$

$$X_{coil} = \frac{-(\omega M_{12})^2 X_{rx}}{(R_{rx} + R_2)^2 + X_{rx}^2} \quad (8)$$

To determine the relationship between mutual inductance and the optimal inverter load, we use the following equations after a lengthy manipulation:

$$R_{tx}^{opt} = \frac{1}{R_2} \frac{1}{\frac{1}{(\omega M)^2} + \sqrt{\frac{1}{(\omega M)^4} + \frac{1}{R_1 R_2} \frac{1}{(\omega M)^2}}} + R_1, \quad (9)$$

$$X_{coil}^{opt} = 0.$$

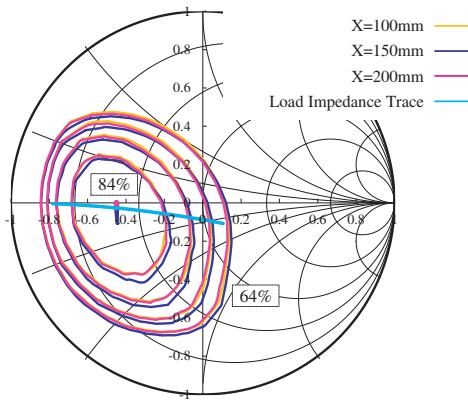


**FIGURE 14.** Load-pull efficiency loci of a full-bridge inverter incorporated with a coil displayed on the Smith chart. Efficiency loci are decreased from 84% to 64%. The input impedance trace of the class-D rectifier is also drawn in black line. Efficiency loci appear almost identical with different receiver (Rx) positions of  $X = 100$  mm, 150 mm, and 200 mm.

From (9), we observe that the optimal inverter load is only affected by the real part of the impedance, which is a function of the mutual inductance ( $M$ ). We design the system to maintain an almost constant mutual inductance to yield a constant value of optimal transmitter resistance.

To verify the system’s efficiency, we simulate the impedance loci for different system efficiencies (84% to 64%) on the Smith chart, as shown in Fig. 14. The input impedance traces (10–100  $\Omega$ ) of the class-D rectifier are also drawn in Fig. 14. Since the system is designed for in-motion operation, we plot the loci for different positions ( $X = 100$  mm, 150 mm, 200 mm) in Fig. 14 as well. Upon detailed observation, we note that the optimal efficiency loci of the receiver coil are almost identical, regardless of its position. This phenomenon is consistent with the prediction of Equation (9). Furthermore, the input impedance trace (10–100  $\Omega$ ) of the class-D rectifier directly passes through the optimal efficiency locus (84%). Therefore, all three modules (inverter, coil, and rectifier) operate at high efficiencies without additional matching circuits.

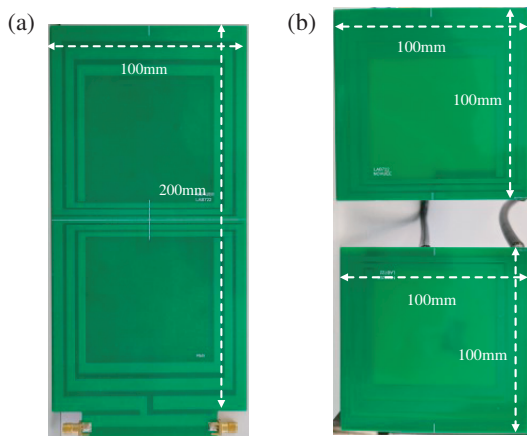


**FIGURE 15.** Fabrication of PCB coils. (a) Transmitter sub-coil. (b) Receiver twin coil.

### 5. MEASUREMENT RESULTS AND DISCUSSIONS

Both the transmitter and receiver coils are fabricated using a printed circuit board made of FR-4, as shown in Fig. 15. To measure the coil resistance, an impedance analyzer (Keysight E4990A) is used at a frequency of 13.56 MHz. The metal resistances of the transmitter and receiver coils are recorded as 1.04  $\Omega$  and 4  $\Omega$ , respectively. The transmitter coil has dimensions of 100 mm · 200 mm, while the receiver coil has dimensions of 2 · 100 mm · 100 mm. The receiver coil is formed by two square coils with opposite current directions, requiring a coaxial cable to be placed across the transmitter coil.

To verify the proposed system, a track and a moving vehicle with a motor are implemented using a 3D printer (Anycubic) to build a demonstration system, as shown in Fig. 16. The 3D printer is used to manufacture the moving coil rail, and the motor is connected to the gear rack to achieve constant speed movement at 70 mm/s.

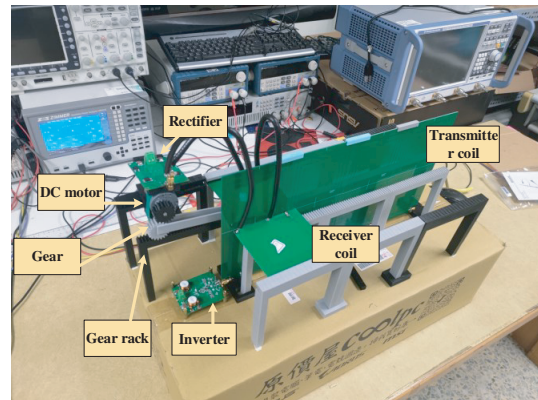


**FIGURE 16.** Measurement environment of the dynamic WPT system.

The inverter drives the four parallel transmitter coils to couple energy to the receiver coil, which generates DC voltage through the rectifier to drive the motor and move the vehicle. The components used in the class-E inverter and class-D rectifier are listed in Table 3. The input voltage ( $V_{DD}$ ) and bias voltage ( $V_{GS}$ ) of the system are 20 V and 5 V, respectively, supplied by a DC power source. The waveforms of the gate and drain terminals of the inverter are shown in Fig. 17(a). When the transistor is turned off, the peak drain voltage ( $V_{DS}$ ) is about 60 V. The non-overlap of drain and gate voltages demonstrates

**TABLE 3.** Components list of inverter and rectifier.

class-E Inverter	
Components	Manufacture/Part
$M_1, M_2$	GaN Systems/GS66504B-MR
$L_{p1}, L_{p2}$	Coilcraft/2014VS-151MEB
$C_{p1}, C_{p2}$	KEMET/CBR06C050FAGAC
class-D Rectifier	
$D_1-D_4$	STMicroelectronics/STPSC8H065B-TR
$C$	TDK/C5750X7S2A156M250KB

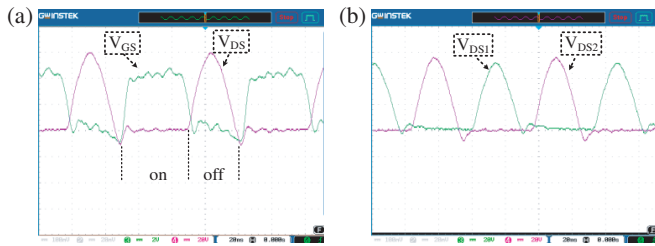


**FIGURE 17.** (a) Measured waveforms of the drain and gate voltages of the transmitter MOS transistor. (b) Full-bridge inverter output voltages of two output terminals.

the switching behavior. The drain voltage of the two transistors of the full-bridge inverter is depicted in Fig. 17(b), with the two waveforms showing almost identical amplitude and no overlap. Hence, the output voltage range ( $V_{DS1}-V_{DS2}$ ) of the transmitter circuit is approximately sinusoidal, eliminating the need for the LC filter in the traditional architecture. The input power, output power, and total efficiency of the system are measured using a power analyzer (LMG640), demonstrating an efficiency and output power of 75.3% and 30.3 W, respectively.

A highly efficient WPT system successfully integrated the transmitter, receiver, and coils, as illustrated in Fig. 18. The overall performance of the system, which comprises these three modules, was represented by the measured DC-DC efficiency. Based on the graph, the total losses of the system were calculated to be approximately 9.94 W. Specifically, the efficiency of the receiver was found to be approximately 96%, corresponding to a loss of around 1.68 W. The efficiency of the coil was obtained by analyzing the measured raw data in Fig. 8. The imaginary part was extracted to derive the mutual inductance, and the real part was used to obtain the coil losses, which were approximately 4.57 W. By combining these losses, the loss of the transmitter was calculated to be approximately 3.66 W. To clearly illustrate these power losses, they were presented as percentages in Fig. 18. The coil remained to be the major loss, accounting for roughly 46.1% of the total losses. Since the system operates at a frequency of 13.56 MHz, coil loss continues to represent a significant proportion of the overall system efficiency.

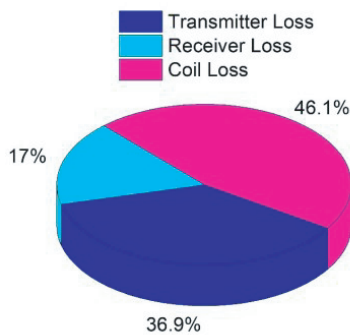


**FIGURE 18.** Power loss percentages of the transmitter, coil and receiver.

Figure 19 shows the output power and efficiency at different receiver positions. When receiver is within the range of the transmitter coil ( $X = 10\text{ mm}-400\text{ mm}$ ), the system effi-

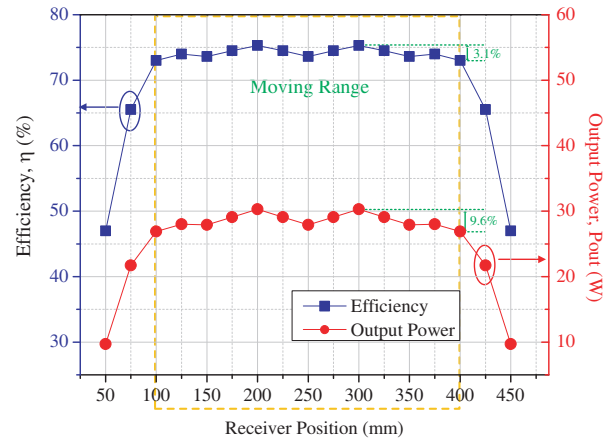


**FIGURE 19.** Measurement results of the proposed WPT system at different receiver coil positions. (a) Efficiency and output power as a function of receiver position. The highest efficiency and output power are achieved when receiver is positioned at  $X = 200\text{ mm}$ , while the output voltage and current are almost constant regardless of the receiver position.

ciency varies from 73% to 75.3%, and the output power varies from 27.5 W to 30.3 W. The measured output voltage ( $V_{out}$ ) and output current ( $I_{out}$ ) are with the average output voltage and current being 34.2 V and 0.84 A, respectively. The variation is less than 6%. Based on previous measurement results, the proposed dynamic WPT system moves at a speed of 70 mm/s and achieves stable output performance at different receiver positions.

Table 4 provides a comparison of our study with other reported works in the MHz frequency range. In [4], a system with four transmitter coils and one receiver coil was used, where each transmitter coil required its own inverter. The length of the receiver coil was optimized to be 1.43 times that of the transmitter coil. The system achieved 80% efficiency with a 10% variation, but additional switch elements were required. In [7, 8], the efficiency variation range is larger than 19%.

**TABLE 4.** Benchmark of the proposed study with reported literature.

Ref.	Output Power Variation	Efficiency Variation Range	Output Power (DC)	Freq. (MHz)	Control Circuits
This work	9.6% (DC)	73%–75.3%	30W	13.56	No
[4]	10% (DC)	70%–84%	100W	6.78	Yes
[7]	70.8% (DC)	65%–84%	120W	0.085	No
[8]		57%–71.6%	2W	13.56	No

\* Power gain formula [13]

In contrast, our study demonstrates stable output power of 30 W with a variation of only 9.6%, achieved by changing the coupling topology without the need for additional compensa-

tion components. The performance is comparable to that of [4]. Moreover, the efficiency variation of our system ranges from 73% to 75.3%, which is well suited for dynamic WPT applications.

## 6. CONCLUSION

In this study, a dynamic WPT system with constant output power was successfully implemented using orthogonal coupling coils. A topology was proposed to solve output power fluctuation by analyzing mutual inductance variation. The coil transmission efficiency was improved by adjusting the coil width. The entire coil buried on the track was built using four parallel sub-coils in the transmitter array, chosen based on component cost.

For the transmitter of the proposed system, a full-bridge class-E inverter operating at 13.56 MHz was used, whereas the receiver used a full-bridge class-D rectifier. The efficiency loci of transmitter and the input impedance trace of receiver were simultaneously drawn on the Smith chart to integrate the three modules of the whole system in the high-efficiency region. It was demonstrated that the output power was independent of the receiver position, and the system's highest efficiency reached 75.3%. The output power remained stable at 30 W, and the variation of different receiver positions was only 9.6%.

Valuable references for designing dynamic WPT systems, especially those requiring stable output power without additional compensation components, were provided by this study. The proposed topology effectively solved the output power fluctuation problem, and the improved coil transmission efficiency further enhanced the system's performance. Overall, the results demonstrated the potential of using orthogonal coupling coils in dynamic WPT systems to achieve high efficiency and stable output power.

## ACKNOWLEDGEMENT

This work was supported by the Microwave Energy Transmission Laboratory (METLAB), Research Institute for Sustainable Humanosphere, Kyoto University and National Institute of Information and Communications Technology (NICT), Grant No. 02401.

## REFERENCES

[1] Cheng, C., F. Lu, Z. Zhou, et al., "A load-independent LCC-compensated wireless power transfer system for multi-

- ple loads with a compact coupler design," *IEEE Trans. Industrial Electronics*, Vol. 67, No. 6, 4507–4515, Jun. 2020, doi: 10.1109/TIE.2019.2931260.
- [2] Xiao, H., H. Zhang, W. Song, J. Wang, W. Chen, and M. Lu, "A high-input power rectifier circuit for 2.45-GHz microwave wireless power transmission," *IEEE Trans. Industrial Electronics*, Vol. 69, No. 3, 2896–2903, Mar. 2022, doi: 10.1109/TIE.2021.3063971.
- [3] Kurs, A., A. Karalis, R. Moffatt, J. D. Joannopoulos, P. Fisher, and M. Soljavci, "Wireless power transfer via strongly coupled magnetic resonances," *Science*, Vol. 317, No. 5834, 83–86, Jul. 2007.
- [4] Pacini, A., A. Costanzo, S. Aldhaher, and P. D. Mitcheson, "Load- and position-independent moving MHz WPT system based on GaN-distributed current sources," *IEEE Trans. Microwave Theory and Techniques*, Vol. 65, No. 12, 5367–5376, Dec. 2017.
- [5] Wu, H. H., G. A. Covic, J. T. Boys, and D. J. Robertson, "A series-tuned inductive-power-transfer pickup with a controllable ac-voltage output," *IEEE Trans. Power Electronics*, Vol. 26, No. 1, 98–109, Jan. 2011.
- [6] Smeets, J. P. C., T. T. Overboom, J. J. Jansen, and E. A. Lomonova, "Comparison of position-independent contactless energy transfer systems," *IEEE Trans. Power Electronics*, Vol. 28, No. 4, 391–399, Apr. 2013.
- [7] Zhou, S. and C. C. Mi, "Multi-paralleled LCC reactive power compensation networks and their tuning method for electric vehicle dynamic wireless charging," *IEEE Trans. Industrial Electronics*, Vol. 63, No. 10, 6546–6556, Oct. 2016, doi: 10.1109/TIE.2015.2512236.
- [8] Xu, C., Y. Zhuang, C. Song, Y. Huang, and J. Zhou, "Dynamic wireless power transfer system with an extensible charging area suitable for moving objects," *IEEE Trans. Microwave Theory and Techniques*, Vol. 69, No. 3, 1896–1905, Mar. 2021.
- [9] Hsu, H.-M., K.-Y. Chan, H.-C. Chien, and H.-C. Kuan, "Analytical design algorithm of planar inductor layout in CMOS technology," *IEEE Trans. Electron Devices*, Vol. 55, No. 11, 32083213, Nov. 2008.
- [10] Dionigi, M., M. Mongiardo, and R. Perfetti, "Rigorous network and full-wave electromagnetic modeling of wireless power transfer links," *IEEE Trans. Microwave Theory and Techniques*, Vol. 63, No. 1, 65–75, Jan. 2015.
- [11] Huang, S.-J., T.-S. Lee, W.-H. Li, and R.-Y. Chen, "Modular on-road AGV wireless charging systems via interoperable power adjustment," *IEEE Trans. Industrial Electronics*, Vol. 66, No. 8, 5918–5928, Aug. 2019.
- [12] Grover, F. W., *Inductance Calculations: Working Formulas and Tables*, Van Nostrand, New York, 1946.
- [13] Pozar, D. M., *Microwave Engineering*, 4th Edition, John Wiley & Sons, 2011.